# Loss of function mutations in *CCDC32* cause a congenital syndrome characterized by craniofacial, cardiac and neurodevelopmental anomalies

Tamar Harel[1,#], John N. Griffin[2,3,#], Thomas Arbogast[2,#], Tanner O. Monroe[4,5], Flavia Palombo[6], Marcella Martinelli[7], Marco Seri[8,9], Tommaso Pippucci[9], Orly Elpeleg[10,*], and Nicholas Katsanis[4,5]*

[1]Department of Genetic and Metabolic Diseases, Hadassah-Hebrew University Medical Center, Jerusalem 91120, Israel.
[2]Center for Human Disease Modeling, Duke University, Durham, NC 27701, USA
[3]School of Biological Sciences, University of East Anglia, Norwich Research Park, Norwich, NR4 7TJ, United Kingdom
[4]Department of Pediatrics, Northwestern University Feinberg School of Medicine, Chicago, IL, 60611, USA.
[5]Advanced Center for Translational and Genetic Medicine (ACT-GeM), Stanley Manne Children's Research Institute, Ann & Robert H. Lurie Children's Hospital of Chicago, 225 East Chicago Avenue, Box 205, Chicago, IL 60611, USA.
[6]IRCCS Institute of Neurological Sciences of Bologna, Bellaria Hospital, 40138 Bologna, Italy
[7]Dipartimento di Medicina Specialistica, Diagnostica e Sperimentale, Università di Bologna, 40138 Bologna, Italy
[8]Dipartimento di Scienze Mediche e Chirurgiche, Università Di Bologna, 40138 Bologna, Italy
[9]U.O. Genetica Medica, Policlinico S. Orsola-Malpighi, Azienda Ospedaliero-Universitaria di Bologna, 40138 Bologna, Italy.
[10]Monique and Jacques Roboh Department of Genetic Research, Hadassah-Hebrew University Medical Center, 91120, Jerusalem, Israel.

1

# These authors contributed equally.

*Correspondence:
elpeleg@hadassah.org.il
nkatsanis@luriechildrens.org

**Abstract**

Despite the wide use of genomics to investigate the molecular basis of rare congenital

malformations, a significant fraction of patients remains bereft of diagnosis. As part of our

continuous effort to recruit and perform genomic and functional studies on such cohorts, we

investigated the genetic and mechanistic cause of disease in two independent consanguineous

families affected by overlapping craniofacial, cardiac, laterality, and neurodevelopmental

anomalies. Using whole exome sequencing, we identified homozygous frameshift *CCDC32*

variants in three affected individuals. Functional analysis in a zebrafish model revealed that

*ccdc32* depletion recapitulates the human phenotypes. Because some of the patient phenotypes

overlap defects common to ciliopathies, we asked if loss of CCDC32 might contribute to the

dysfunction of this organelle. Consistent with this hypothesis, we show that *ccdc32* is required

for normal cilia formation in zebrafish embryos and mammalian cell culture, arguing that ciliary

defects are at least partially involved in the pathomechanism of this disorder.

**Introduction**

Discovered in 1675, cilia were among the first described cellular organelles and are now understood to be present near ubiquitously in vertebrate cells. However, it is only in the last two decades that intensive genetic and molecular discovery has revealed the extent of the influence of cilia on human development and health (1-3). Cilia are complex microtubule-based appendages that provide both motile force and mediate reception and transduction of extracellular signals. Mutations that affect cilia structure and/or function can impair embryogenesis and underlie a constellation of congenital diseases, unified under the broad ciliopathy umbrella(4). These disorders often share phenotypic features (e.g. craniofacial, laterality, cerebral, retinal, renal, skeletal, and fertility abnormalities), but vary in their clinical presentation and severity (2, 3, 5).

Cilia production and function are complex and regulated, requiring the coordinated action of proteins and cellular processes(1, 6). While the contribution of ciliary dysfunction to human disease is clear, the heterogeneity of cilia genetics, structure, and function challenges our understanding of disease mechanism, and hampers our ability to diagnose affected families. Thus, the continued discovery of ciliary genes and disease variants is a critical step in improving our ability to identify and treat ciliopathies.

Here, we examined individuals from two independent consanguineous families affected by overlapping clinical features suggestive of a ciliopathy that include craniofacial, cardiac, laterality and neurodevelopmental anomalies. We report that both individuals carry homozygous frameshift variants in *CCDC32*, a locus hitherto unknown to be involved with human pathology. Furthermore, we show that CRISPR–Cas9 mediated deletion of *ccdc32* in zebrafish impaired

3

embryonic cilia formation and recapitulated key human phenotypes. Together, our data extend the causal recessive loci for this group of disorders to include variants in *CCDC32*.

**Results**

Family A (Figure 1A, Table S1), a consanguineous Arab Muslim pedigree (first cousins, once removed), includes a six-year-old female (Individual A-II-1) who presented with global developmental delay, feeding difficulties in infancy, and congenital anomalies including cleft lip and palate, atrioventricular (AV) canal defect, and abdominal situs inversus with asplenia. Physical examination revealed borderline microcephaly (3$^{rd}$-5$^{th}$ percentile), height at 80$^{th}$ percentile, and weight at 32$^{nd}$ percentile. Dysmorphic features included hypotelorism, upslanting palpebral fissures, a stiff upper lip, missing teeth attributed to the clefting, vaulted palate with cleft, prominent ears, underdeveloped helices, and micrognathia. She had mild kyphosis and nail clubbing; abnormal dermatoglyphics, bilateral camptodactyly, and clinodactyly of the fifth fingers. Brain MRI revealed hypoplastic cerebellar tonsils. Ophthalmology, audiology and renal evaluations were within normal limits. A sibling fetus in Family A (A-II-2) had bilateral cleft lip, vermian hypoplasia, hypoplastic pons, and abnormal cisterna magna that were detected by ultrasound, and the pregnancy was terminated electively. No heart defect was detected in the fetus. Chromosomal microarray (CMA) of both individuals was normal.

We also independently consulted Family B, which included a three-year-old male individual born to first cousins of Iranian-Isfahan descent (Individual B-II-1) with no known family history of congenital anomalies. At birth, individual B-II-1 weighed 3.1kg and presented with bilateral cleft lip, cleft palate, ventricular septal defect and pulmonary valve stenosis. He had severe

4

feeding difficulties, moderately delayed motor and language development, and hyperactivity. Physical examination revealed microcephaly (Z score -2.5), height at 97th percentile, and weight at 64th percentile. Dysmorphic features included brachydactyly, hypertelorism, epicanthal folds, broad nasal root, a prominent large nose, and malformed protruded ears. The individual had clinodactyly; nail aplasia on thumbs and toes; and cryptorchidism. Other evaluations, including ophthalmology, electroencephalogram (EEG), and renal ultrasound were normal. Detailed clinical findings of all affected individuals are summarized in **Supplemental Table 1**.

With informed consent from each of our institutions, probands from Family A and Family B (**Figure 1A**) underwent whole exome sequencing (WES) in search of an underlying molecular diagnosis. Genomic DNA samples from Family A were collected using the SureSelect Human All Exon 50 Mb V5 Kit (Agilent Technologies), while samples from Family B were captured with Nextera Rapid Capture Exome and Expanded Exome Kits. DNA libraries from families A and B were sequenced on HiSeq2500 and HiSeq2000 platforms (Illumina), respectively. Reads were aligned to the reference human genome assembly hg19 (GRCh37) and the mean coverage was 71X for Family A and 58X for Family B. Variants were called as described(7, 8) and in accordance with GATK recommendations. For Family A, variants were filtered out if the total read depth was less than 7X, and if they were off-target, synonymous, or had minor allele frequency (MAF) >0.01 in the in-house and dbSNP databases, or MAF >0.005 in the GnomAD database. Nine homozygous variants survived filtering (**Supplemental Table 2**). For Family B, Runs of Homozygosity (ROH) were detected from WES data with H3M2(9), and the analysis focused on homozygous variants within large regions of homozygosity (ROH >= 1.5 Mb) which are the most likely to be identical by descent(10). We retained only variants predicted to affect

5

protein function (nonsynonymous, nonsense, splicing and small indels), and we filtered out

variants with a minor allele frequency greater than 0.01 or that appeared to be homozygous in the

gnomAD, EVS, 1000 Genomes or in the Bologna in-house database, including about >1000

additional WES samples. Analysis of WES data was made on the assumption of a recessive

inheritance pattern on the basis of consanguinity (families A and B), and multiple affected

members (family A). No biallelic variants were identified in genes known to cause Mendelian

diseases overlapping the affected individuals' phenotypes. Validation and segregation studies of

variants of interest was performed by Sanger sequencing.

Homozygous frameshift variants in *CCDC32,* which encodes a 194 amino acid polypeptide of

unknown function, were identified in both families. In Family A, a homozygous frameshift

variant (chr15:g.40855188dupA [hg19]; NM_001080791.2: c.54dupT, p.(Thr19Tyrfs*12)),

mapping within a ~9.06Mb ROH, segregated with the disease in available family members

(**Figure 1A**). This variant is predicted to produce a premature termination codon (PTC) at

position 30 and was absent from gnomAD, TOPMed, Geno2MP, and the GME Variome. In

Family B, only one homozygous variant survived the aforementioned bioinformatic filtering: a

homozygous dinucleotide insertion (chr15:g.40855052dupCC; NM_001080791.2;

c.189_190dupGG: p.Glu64Glyfs*12), mapping within a 5.23 Mb ROH. The frameshift insertion

was confirmed by Sanger sequencing as bi-allelic with each allele segregating from one of the

parents (**Figure 1A**). Discovery of these two families was facilitated by GeneMatcher(11).

As the biological role of *CCDC32* is unknown, we next used CRISPR-Cas9 technology to model

*ccdc32* depletion *in vivo* and to further investigate its potential contribution to the observed

6

clinical phenotype. Zebrafish is a useful model for such studies as each mating produces

hundreds of genetically tractable, externally developing embryos, allowing rapid and efficient

investigation of gene function in development and initial testing of causality of newly-discovered

disease loci at a scale and cost that is able to address the needs of genomic discovery (12). For

example, aspects of craniofacial, neurological and cardiac development can readily be assessed

within three days of manipulating fertilized eggs and they have been paired to our discovery

sequencing studies of congenital structural defects of unknown etiology (13-18). A single

ortholog of *CCDC32* exists in the zebrafish genome (46% identity, 64% similarity). We designed

two distinct single guide (sg)RNAs (sgRNA1 and sgRNA2) targeting non-overlapping regions of

exon 2 of *ccdc32* and injected each into zebrafish embryos at the one cell stage, along with Cas9

protein. We evaluated the efficacy of our *ccdc32* gene editing by heteroduplex analysis, cloning,

and sequencing of sgRNA targeted regions(13, 15, 19), which revealed an average of 85%

(sgRNA1) and 70% (sgRNA2) mosaic alterations in F0 crispants (**Supplemental Figure 1**).

As all three affected individuals exhibited overlapping craniofacial and neurodevelopmental

abnormalities, including microcephaly, midline facial defects, and cerebellar hypoplasia, we first

examined the development of analogous structures in our zebrafish model. Editing of *ccdc32*

with either sgRNA resulted in a significant reduction in head size at 3 dpf compared to either

uninjected or sgRNA-only (no CAS9 protein) injected controls, recapitulating the human

microcephaly phenotype (**Figure 2A**). Furthermore, *ccdc32* crispants exhibited significant,

reproducible alterations in facial skeletal morphology compared to controls, as measured by the

angle of the bilateral ceratohyal cartilages (**Figure 2B**).  Immunostaining with anti-α-acetylated

tubulin also revealed hypoplastic cerebella in *ccdc32*-depleted larvae (**Figure 2C**). Importantly,

development of the CRISPR modified larvae was not globally delayed as no reduction in overall

body length was detected (**Supplemental Figure 2**), a finding consistent with our recent

observations of trivial background off-target mutations in mosaic crispants (20).

Congenital heart anomalies were patent in both probands, and individual A-II-1 exhibited

heterotaxy. To test whether *ccdc32* is required for embryonic axis development, we examined

left/right development in our crispant embryos. In vertebrates, left/right symmetry is first broken

at an organizing center: the node in mouse or Kupffer's vesicle (KV) in zebrafish(21, 22). Here,

motile cilia produce a directional fluid flow across the organizer which is subsequently translated

by primary cilia into asymmetric expression of developmentally important genes and normal

organ placement(5, 21-26). Organ situs, in particular cardiac looping, can be examined readily in

zebrafish embryos due to their optical transparency, availability of transgenic reporters, and

external development. Depletion of *ccdc32* using either of our sgRNAs disrupted cardiac looping

at 2 dpf (**Figure 3A**), demonstrating that *ccdc32* plays a required and conserved role in

vertebrate left - right symmetry breakage. We further noted that expression of southpaw (*spaw)*,

a key left/right patterning transcript, was impaired in our *ccdc32* crispants at the 18 somite stage

(**Figure 3B**), suggesting that *ccdc32* functions at an early stage of axis development. Consistent

with this notion, *ccdc32* transcripts were detected as early as one hour post fertilization in

zebrafish development, and were particularly localized to the developing head and neural tube

throughout embryogenesis, including the KV region (**Supplemental Figure 3**).

To explore a potential role for *ccdc32* in KV development, we next examined *ccdc32*

requirements in cilia formation in the zebrafish KV. Immunostaining with anti-α-acetylated

tubulin revealed that KV cilia were reduced significantly in both number and length in crispants at the 10 somite stage (**Figure 4A**). Cilia formation was similarly impaired in ciliated mouse inner medullary collecting duct cells with GFP labelled cilia (IMCD3 5-HT6-GFP) following siRNA-mediated knockdown of *Ccdc32* (**Figure 4B**). Together, these data suggest that *ccdc32* plays an evolutionarily conserved role in the formation and/or maintenance of cilia in the vertebrate left/right organizing center and is required for normal left/right axis development.

**Discussion**

Our clinical and animal modeling data demonstrate that homozygous mutations in *CCDC32* likely cause a congenital syndrome characterized by craniofacial, cardiac and neurodevelopmental anomalies. These variants segregate in an autosomal-recessive paradigm in the pedigrees examined in this study.

Cilia fulfil diverse motility and sensory functions in embryogenesis, including the mediation of critical signaling pathways such as Shh, $Ca^{2+}$, and PCP (2, 3). Unsurprisingly, a broad range of developmental phenotypes are commonly associated with impaired cilia function, including craniofacial, laterality, cerebral, and splenic abnormalities (4). Our functional analyses in zebrafish reveal that ccdc32 depletion impairs cilia formation and demonstrate a contribution of *ccdc32* in craniofacial, brain and left/right axis development, broadly recapitulating our patient phenotypes. While the reduction in KV cilia patent in our CRISPR targeted embryos is mild, this might reflect the mosaic nature of our F0 knockdown and/or the persistence of maternal transcript at early stages. In future studies it will be of interest to examine the severity of the cilia phenotype in later developmental contexts, as well as in null zebrafish lines. While we cross-

9

validated the cilia phenotype in a mammalian cell line, production of a complimentary

mammalian model would enable a more complete model of the clinical phenotypes which are

challenging to recapitulate in the zebrafish model (cleft lip and palate, certain cardiac

malformations and digit abnormalities). Finally, we note that, while there is variation in the

number and length of KV cilia, our findings are comparable in severity with previous zebrafish

studies that link modest impairment of ciliogenesis to defective left/right patterning *(27-29)*.

Together, our data suggest an evolutionary conserved role for *CCDC32* in cephalic and left/right

axis development and support a ciliary contribution to the pathomechanism of the patient

phenotypes. Whether this molecule also performs non-ciliary roles relevant to the human

pathology remain unclear.

While our data suggests a role for *CCDC32* in ciliogenesis, the molecular function of the

encoded protein remains undefined. CCDC32 has been reported to interact with the C-terminal

of annexin A2, a calcium-dependent phospholipid-binding protein involved in myriad cellular

process including membrane-cytoskeleton interactions, membrane trafficking, signal

transduction and proliferation (30-32), however the functional significance of this interaction is

unknown. We and others have also reported previously that CCDC proteins are enriched in the

ciliary proteome (33-35), and we note that other CCDC genes have been associated with cilia

function and disease. For example, mutations in *CCDC39* [MIM 613798], *CCDC40* [MIM

613799], *CCDC103* [MIM 614677], and *CCDC114* [MIM 615038] affect cilia motility and

cause primary ciliary dyskinesia [MIM 244400] (36-41). This is consistent with our functional

hypothesis that *CCDC32* contributes to a ciliary function and with the clinical presentation of

features pathognomonic of ciliopathies. At the same time, some of the hallmark ciliopathy

10

pathologies were absent from the described individuals, such as cystic renal disease and polydactyly. These observations might be explained either by the specificity of CCDC32 function or the presence of *cis* and *trans* allele-specific exacerbating or suppressive genetic interactions that are well-documented for this group of disorders (42). Further investigation is required to test a direct function for CCDC32 in cilia formation and advance our understanding of the human syndrome.

**Materials and Methods**

*Human Subjects Recruitment and Ethics*

Informed consent was obtained from Family A for participation in the research study, according to IRB-approved protocol 0306-10-HMO, and for Family B according to IR-MUI-MED-REC protocol.

*Exome analysis*

Family A: Following informed consent, whole exome sequencing (WES) was pursued on DNA extracted from whole blood of individual II-1 of Family A (Fig. 1A). Exonic sequences of DNA were enriched with the SureSelect Human All Exon 50 Mb V5 Kit (Agilent Technologies, Santa Clara, California, USA). Sequences were generated on a HiSeq2500 (Illumina, San Diego, California, USA) as 125-bp paired-end runs. Read alignment and variant calling were performed with DNAnexus (Palo Alto, California, USA) using default parameters with the human genome assembly hg19 (GRCh37) as reference. Exome analysis of the probands yielded 48.6 million mapped reads, with a mean coverage of 71X. Candidate genes were entered into

11

GeneMatcher(11), a freely accessible website designated to facilitate collaboration between clinicians and researchers with an interest in the same gene.

Family B: Subject II-1 of Family B (Fig. 1A) underwent WES as part of a cohort of ~60 children with suspected genetic disorders and consanguineous parents. Following informed consent, DNA from whole blood was captured using the Nextera Rapid Capture Exome and Expanded Exome Kits (Illumina Inc., San Diego, CA, USA) and sequenced as 100 bp paired-end reads on an Illumina HiSeq2000 platform (Illumina Inc., San Diego, CA, USA). Generated reads were treated following a general workflow for variant calling as elsewhere reported(7). Generated reads were checked with FastQC (http://www.bioinformatics.babraham.ac.uk/publications.html) and aligned with BWA(43) to the reference genome hg19. Aligned reads were treated for realignment and base quality score recalibration with GATK(44) and for duplicate removal with PicardTools (http://picartools.sourceforge.net). Alignment statistics were collected by SAMtools(45) and GATK. Coverage statistics over the targeted regions were calculated with GATK. Variant calling and filtering by quality were performed by GATK. Variants passing quality filters were annotated with Ensembl Variant Effect Predictor (VEP) (http://www.ensembl.org/). Sanger sequencing was used to confirm the identified variants and test the carrier status of unaffected family members. H3M2(9) was used for the identification of ROHs from WES alignments.

*Segregation analysis*

Amplicons containing the *CCDC32* variants were amplified by conventional PCR of genomic DNA, and analyzed by Sanger dideoxy nucleotide sequencing.

*Fish breeding and maintenance*

12

All zebrafish experiments where performed in accordance with Duke University institutional animal care and use committee (IACUC) protocols. Embryos were obtained by natural mating of adult zebrafish of the ZDR background or carrying the *-1.4col1a1:egfp* transgenic reporter. Embryos were grown in egg water (0.3 g/L NaCl, 75 mg/L CaSO4, 37.5 mg/L NaHC03, 0.003% methylene blue) at 28°C until collected at 1 or 3 days post-fertilization [dpf].

*CRISPR/Cas9 genome editing in zebrafish embryos*

To deplete *ccdc32*, we used CHOPCHOP to identify 2 guide RNA (gRNA) first 5'-GCTAAAGTTAGCAGCTCTGG-3' and second 5'-ACCCACGCGGCCCGATCTAG-3' targeting exon 2. gRNA was transcribed *in vitro* using the GeneArt precision gRNA synthesis kit (Thermo Fisher Scientific) according to the manufacturer's instructions. 1 nl of injection cocktail containing 100 pg/nl gRNA and 200 pg/nl Cas9 protein (PNA Bio, Thousand Oaks, CA) was injected into the cell of embryos at the 1-cell stage. To determine targeting efficiency in founder (F0) mutants, we extracted genomic DNA from 2 day post-fertilization (dpf) embryos and PCR amplified the region flanking the gRNA target site using primers firstF: 5'-TACGCGTGTAAACAGCAAACTT-3' and firstR: 5'-CAGGGTACCATGCACTTACAAA-3' and secondF: 5'-TTACGCGTGTAAACAGCAAACT-3' and secondR: 5'-CAGGGTACCATGCACTTACAAA-3'. PCR products were denatured, reannealed slowly and separated on a 20% TBE 1.0-mm precast polyacrylamide gel (Thermo Fisher Scientific), which was then incubated in ethidium bromide and imaged on a ChemiDoc system (Bio-Rad, Hercules, CA) to visualize hetero- and homoduplexes. To estimate the percentage of mosaicism of *ccdc32* F0 mutants (n = 5/condition), PCR products were gel purified (Qiagen, Germantown, MD), and cloned into the pCR8/GW/TOPO-TA vector (Thermo Fisher Scientific). Plasmid was prepped

13

from individual colonies (n=10–12 colonies/embryo) and Sanger sequenced according to standard procedures.

*In Situ Hybridization*

*In-situ* hybridization was performed as described[7]. The RNA probe for *ccdc32* was designed to detect a 557 bp region, including the 3' UTR. Sense and antisense reverse-transcription template DNA was created by PCR amplifying WT zebrafish cDNA using primers that added T7 and T3 RNA polymerase promoters (underlined) to the 5' and 3' ends (F:5'<u>TAATACGACTCACTATAGGGAGA</u>TTTGATCAGAGTGCTTTGGAGC3'; R:5'<u>AATTAACCCTCACTAAAGGGAGA</u>TTCATGGATGCACCGTTTAGC3'). RNA probes were synthesized to include digoxigenin (Roche #11745816910) using either T3 (Roche #11031163001) or T7 (Promega # P2075) RNA polymerase, and detected using standard anti-digoxigenin (Roche #11093274910), NBT/BCIP detection (Roche # 11681451001). Digoxingenin labeled anti-sense RNA probe for *spaw* riboprobes (a kind gift from Drs Kenneth D Poss and Michel Bagnat, Duke University) was made using a T7 mMessage mMachine transcription kit (Ambion #AM1344).

*Whole Mount Immunostaining*

Immunostaining was performed as described previously. 3 dpf embryos were fixed overnight in Dent's solution (80% methanol, 40% DMSO), dehydrated in methanol, and rehydrated through a graded series of PBST in methanol washes. They were bleached for 10 min in 9mL PBST + 1mL $H_2O_2$ + 0.05 g KOH and washed three times for 10 min each in PBST. Embryos were permeabilized with proteinase K for 10 min, then incubated overnight in primary antibody (anti-

14

α-acetylated tubulin, 1:1,000 Sigma-Aldrich, T7451). Following three washes in PBST, embryos were incubated with secondary antibody (Alexa Fluor 488 goat anti-rabbit IgG, 1:500, Thermo Fisher Scientific, A11001) for 2 h and washed three times with immunofluorescence (IF) buffer (1% BSA in PBST).

*Automated zebrafish imaging*

3 dpf zebrafish *-1.4col1a1:egfp* transgenic embryos were collected and automatic imaging was conducted with an AxioScope.A1 microscope and Axiocam 503 monochromatic camera facilitated by Zen Pro software (Zeiss), to capture dorsal images of GFP signal. Larval batches were positioned and imaged live using the Vertebrate Automated Screening Technology (VAST; software version 1.2.5.4; Union Biometrica) BioImager. Larvae from each experimental condition were anesthetized with 0.2 mg/mL Tricaine prior to being loaded into the sample reservoir. Dorsal and lateral image templates of uninjected controls and experimental larvae were created and we acquired images at a >70% minimum similarity for the pattern-recognition algorithms. Larvae were rotated to 180° to acquire ventral images via a 10x objective and fluorescent excitation at 470nm to detect GFP to capture fluorescent images of the pharyngeal skeleton. ImageJ software (NIH) was used to measure the angle of the ceratohyal cartilage. All experimental conditions were normalized to uninjected controls and set to 100 degrees. Statistical comparisons were performed using one-way ANOVA with Tukey's test (GraphPad Prism).

*Ccdc32 knockdown in mIMCD3 cells*

15

Mouse inner medullary collecting duct cells containing fluorescent cilia (mIMCD3 5-HT6-GFP) were maintained in DMEM/F12 media (Gibco # 1133003), supplemented with 10% FBS and allowed to attach for 24 hours. When they reached 70% confluency, they were transfected with siRNAs against *Ccdc32* or a nontargeting control (Silencer Select siRNAs ID:s203118, Ambion #4390771, UCACUUGACUGAUCCAUUCta; Silencer Select Negative Control No. 1 siRNA #4390843) at 5nM final concentration. 24 hours after transfection, the media was replaced with serum-free media to induce ciliogenesis. After 24 hours of serum starvation, the cells were either fixed in 10% formalin for imaging (10 minutes, room temperature) or harvested in TRIzol Reagent (Invitrogen #15596026) for gene expression data. qRT-PCR was performed using three sets of primers spanning the exon 1-2 junction (Pair1 F: GCTGGGCAGCTCCAGATGA, R: TGCTGTATGGCTTTCCCCTG; Pair2 F: CTGCTGGGCAGCTCCAGAT, R:GCTGCTGCTGTATGGCTTTC: Pair3 F: CTGGGCAGCTCCAGATGA, R: AGTCTGCTGCTGCTGTATGG), and the results were averaged using three technical replicates and three biological replicates. Nontargeted siRNA and siCCDC32 values are normalized to untreated control cells. Fluorescent cilia were imaged on a Zeiss LSM 880 confocal microscope, and cilia length was measured manually using ImageJ. A total of 4 replicates were imaged for each condition, greater than 500 cells per replicate were imaged, and more than 1000 cilia were measured for each condition. The person imaging and measuring the cilia was blinded to experimental condition.

*Statistical analysis*

Embryos were selected randomly from a fertilized population and utilized for injections, scoring or collection. We estimated 20–25 samples per experimental condition were necessary for

16

statistical significance given the magnitude of the changes expected, and sample size is reported

for each experiment. Each experiment was performed a minimum of 3 times. The statistical

significance of each experiment in figure 2 was examined using a one-way ANOVA with Tukey's

test (GraphPad Prism).

## Acknowledgments

## Conflict of Interest Statement

N.K. holds stock in, and is a paid consultant of Rescindo Therapeutics. The other authors declare

no competing interests.

## References

1 Heydeck, W., Fievet, L., Davis, E.E. and Katsanis, N. (2018) The complexity of the cilium: spatiotemporal diversity of an ancient organelle. *Curr Opin Cell Biol*, **55**, 139-149.
2 Gerdes, J.M., Davis, E.E. and Katsanis, N. (2009) The vertebrate primary cilium in development, homeostasis, and disease. *Cell*, **137**, 32-45.
3 Reiter, J.F. and Leroux, M.R. (2017) Genes and molecular pathways underpinning ciliopathies. *Nat Rev Mol Cell Biol*, **18**, 533-547.
4 Badano, J.L., Mitsuma, N., Beales, P.L. and Katsanis, N. (2006) The ciliopathies: an emerging class of human genetic disorders. *Annu Rev Genomics Hum Genet*, **7**, 125-148.
5 Brueckner, M. (2007) Heterotaxia, congenital heart disease, and primary ciliary dyskinesia. *Circulation*, **115**, 2793-2795.
6 Mirvis, M., Stearns, T. and James Nelson, W. (2018) Cilium structure, assembly, and disassembly regulated by the cytoskeleton. *Biochem J*, **475**, 2329-2353.
7 Pippucci, T., Licchetta, L., Baldassari, S., Palombo, F., Menghi, V., D'Aurizio, R., Leta, C., Stipa, C., Boero, G., d'Orsi, G. *et al.* (2015) Epilepsy with auditory features: A heterogeneous clinico-molecular disease. *Neurol Genet*, **1**, e5.

8 Ta-Shma, A., Zhang, K., Salimova, E., Zernecke, A., Sieiro-Mosti, D., Stegner, D., Furtado, M., Shaag, A., Perles, Z., Nieswandt, B. *et al.* (2017) Congenital valvular defects associated with deleterious mutations in the PLD1 gene. *J Med Genet*, **54**, 278-286.

9 Magi, A., Tattini, L., Palombo, F., Benelli, M., Gialluisi, A., Giusti, B., Abbate, R., Seri, M., Gensini, G.F., Romeo, G. *et al.* (2014) H3M2: detection of runs of homozygosity from whole-exome sequencing data. *Bioinformatics*, **30**, 2852-2859.

10 Pemberton, T.J., Absher, D., Feldman, M.W., Myers, R.M., Rosenberg, N.A. and Li, J.Z. (2012) Genomic patterns of homozygosity in worldwide human populations. *Am J Hum Genet*, **91**, 275-292.

11 Sobreira, N., Schiettecatte, F., Boehm, C., Valle, D. and Hamosh, A. (2015) New tools for Mendelian disease gene identification: PhenoDB variant analysis module; and GeneMatcher, a web-based tool for linking investigators with an interest in the same gene. *Hum Mutat*, **36**, 425-431.

12 Zaghloul, N.A. and Katsanis, N. (2011) Zebrafish assays of ciliopathies. *Methods Cell Biol*, **105**, 257-272.

13 Ansar, M., Ullah, F., Paracha, S.A., Adams, D.J., Lai, A., Pais, L., Iwaszkiewicz, J., Millan, F., Sarwar, M.T., Agha, Z. *et al.* (2019) Bi-allelic Variants in DYNC1I2 Cause Syndromic Microcephaly with Intellectual Disability, Cerebral Malformations, and Dysmorphic Facial Features. *Am J Hum Genet*, **104**, 1073-1087.

14 Khan, K., Zech, M., Morgan, A.T., Amor, D.J., Skorvanek, M., Khan, T.N., Hildebrand, M.S., Jackson, V.E., Scerri, T.S., Coleman, M. *et al.* (2019) Recessive variants in ZNF142 cause a complex neurodevelopmental disorder with intellectual disability, speech impairment, seizures, and dystonia. *Genet Med*, **21**, 2532-2542.

15 Khan, T.N., Khan, K., Sadeghpour, A., Reynolds, H., Perilla, Y., McDonald, M.T., Gallentine, W.B., Baig, S.M., Task Force for Neonatal, G., Davis, E.E. *et al.* (2019) Mutations in NCAPG2 Cause a Severe Neurodevelopmental Syndrome that Expands the Phenotypic Spectrum of Condensinopathies. *Am J Hum Genet*, **104**, 94-111.

16 Reijnders, M.R.F., Kousi, M., van Woerden, G.M., Klein, M., Bralten, J., Mancini, G.M.S., van Essen, T., Proietti-Onori, M., Smeets, E.E.J., van Gastel, M. *et al.* (2017) Variation in a range of mTOR-related genes associates with intracranial volume and intellectual disability. *Nat Commun*, **8**, 1052.

17 Perles, Z., Moon, S., Ta-Shma, A., Yaacov, B., Francescatto, L., Edvardson, S., Rein, A.J., Elpeleg, O. and Katsanis, N. (2015) A human laterality disorder caused by a homozygous deleterious mutation in MMP21. *J Med Genet*, **52**, 840-847.

18 Stankiewicz, P., Khan, T.N., Szafranski, P., Slattery, L., Streff, H., Vetrini, F., Bernstein, J.A., Brown, C.W., Rosenfeld, J.A., Rednam, S. *et al.* (2017) Haploinsufficiency of the Chromatin Remodeler BPTF Causes Syndromic Developmental and Speech Delay, Postnatal Microcephaly, and Dysmorphic Features. *Am J Hum Genet*, **101**, 503-515.

19 Tsai, I.C., McKnight, K., McKinstry, S.U., Maynard, A.T., Tan, P.L., Golzio, C., White, C.T., Price, D.J., Davis, E.E., Amrine-Madsen, H. *et al.* (2018) Small molecule inhibition of RAS/MAPK signaling ameliorates developmental pathologies of Kabuki Syndrome. *Sci Rep*, **8**, 10779.

20 Mooney, M.R., Davis, E.E. and Katsanis, N. (2019) Analysis of Single Nucleotide Variants in CRISPR-Cas9 Edited Zebrafish Exomes Shows No Evidence of Off-Target Inflation. *Front Genet*, **10**, 949.

18

21  McGrath, J., Somlo, S., Makova, S., Tian, X. and Brueckner, M. (2003) Two populations of node monocilia initiate left-right asymmetry in the mouse. *Cell*, **114**, 61-73.

22  Tabin, C.J. and Vogan, K.J. (2003) A two-cilia model for vertebrate left-right axis specification. *Genes Dev*, **17**, 1-6.

23  Nonaka, S., Tanaka, Y., Okada, Y., Takeda, S., Harada, A., Kanai, Y., Kido, M. and Hirokawa, N. (1998) Randomization of left-right asymmetry due to loss of nodal cilia generating leftward flow of extraembryonic fluid in mice lacking KIF3B motor protein. *Cell*, **95**, 829-837.

24  Kawasumi, A., Nakamura, T., Iwai, N., Yashiro, K., Saijoh, Y., Belo, J.A., Shiratori, H. and Hamada, H. (2011) Left-right asymmetry in the level of active Nodal protein produced in the node is translated into left-right asymmetry in the lateral plate of mouse embryos. *Dev Biol*, **353**, 321-330.

25  Schweickert, A., Vick, P., Getwan, M., Weber, T., Schneider, I., Eberhardt, M., Beyer, T., Pachur, A. and Blum, M. (2010) The nodal inhibitor Coco is a critical target of leftward flow in Xenopus. *Curr Biol*, **20**, 738-743.

26  Vonica, A. and Brivanlou, A.H. (2007) The left-right axis is regulated by the interplay of Coco, Xnr1 and derriere in Xenopus embryos. *Dev Biol*, **303**, 281-294.

27  Neugebauer, J.M., Amack, J.D., Peterson, A.G., Bisgrove, B.W. and Yost, H.J. (2009) FGF signalling during embryo development regulates cilia length in diverse epithelia. *Nature*, **458**, 651-654.

28  Frikstad, K.M., Molinari, E., Thoresen, M., Ramsbottom, S.A., Hughes, F., Letteboer, S.J.F., Gilani, S., Schink, K.O., Stokke, T., Geimer, S. *et al.* (2019) A CEP104-CSPP1 Complex Is Required for Formation of Primary Cilia Competent in Hedgehog Signaling. *Cell Rep*, **28**, 1907-1922 e1906.

29  Lin, C.Y., Tsai, M.Y., Liu, Y.H., Lu, Y.F., Chen, Y.C., Lai, Y.R., Liao, H.C., Lien, H.W., Yang, C.H., Huang, C.J. *et al.* (2017) Klf8 regulates left-right asymmetric patterning through modulation of Kupffer's vesicle morphogenesis and spaw expression. *J Biomed Sci*, **24**, 45.

30  Li, Q., Laumonnier, Y., Syrovets, T. and Simmet, T. (2011) Yeast two-hybrid screening of proteins interacting with plasmin receptor subunit: C-terminal fragment of annexin A2. *Acta Pharmacol Sin*, **32**, 1411-1418.

31  Hayes, M.J., Shao, D.M., Grieve, A., Levine, T., Bailly, M. and Moss, S.E. (2009) Annexin A2 at the interface between F-actin and membranes enriched in phosphatidylinositol 4,5,-bisphosphate. *Biochim Biophys Acta*, **1793**, 1086-1095.

32  Grieve, A.G., Moss, S.E. and Hayes, M.J. (2012) Annexin A2 at the interface of actin and membrane dynamics: a focus on its roles in endocytosis and cell polarization. *Int J Cell Biol*, **2012**, 852430.

33  Gherman, A., Davis, E.E. and Katsanis, N. (2006) The ciliary proteome database: an integrated community resource for the genetic and functional dissection of cilia. *Nat Genet*, **38**, 961-962.

34  Ishikawa, H., Thompson, J., Yates, J.R., 3rd and Marshall, W.F. (2012) Proteomic analysis of mammalian primary cilia. *Curr Biol*, **22**, 414-419.

35  Mick, D.U., Rodrigues, R.B., Leib, R.D., Adams, C.M., Chien, A.S., Gygi, S.P. and Nachury, M.V. (2015) Proteomics of Primary Cilia by Proximity Labeling. *Dev Cell*, **35**, 497-512.

36  Antony, D., Becker-Heck, A., Zariwala, M.A., Schmidts, M., Onoufriadis, A., Forouhan, M., Wilson, R., Taylor-Cox, T., Dewar, A., Jackson, C. *et al.* (2013) Mutations in CCDC39 and CCDC40 are the major cause of primary ciliary dyskinesia with axonemal disorganization and absent inner dynein arms. *Hum Mutat*, **34**, 462-472.

37 Becker-Heck, A., Zohn, I.E., Okabe, N., Pollock, A., Lenhart, K.B., Sullivan-Brown, J., McSheene, J., Loges, N.T., Olbrich, H., Haeffner, K. *et al.* (2011) The coiled-coil domain containing protein CCDC40 is essential for motile cilia function and left-right axis formation. *Nat Genet*, **43**, 79-84.

38 Knowles, M.R., Leigh, M.W., Ostrowski, L.E., Huang, L., Carson, J.L., Hazucha, M.J., Yin, W., Berg, J.S., Davis, S.D., Dell, S.D. *et al.* (2013) Exome sequencing identifies mutations in CCDC114 as a cause of primary ciliary dyskinesia. *Am J Hum Genet*, **92**, 99-106.

39 Merveille, A.C., Davis, E.E., Becker-Heck, A., Legendre, M., Amirav, I., Bataille, G., Belmont, J., Beydon, N., Billen, F., Clement, A. *et al.* (2011) CCDC39 is required for assembly of inner dynein arms and the dynein regulatory complex and for normal ciliary motility in humans and dogs. *Nat Genet*, **43**, 72-78.

40 Onoufriadis, A., Paff, T., Antony, D., Shoemark, A., Micha, D., Kuyt, B., Schmidts, M., Petridi, S., Dankert-Roelse, J.E., Haarman, E.G. *et al.* (2013) Splice-site mutations in the axonemal outer dynein arm docking complex gene CCDC114 cause primary ciliary dyskinesia. *Am J Hum Genet*, **92**, 88-98.

41 Panizzi, J.R., Becker-Heck, A., Castleman, V.H., Al-Mutairi, D.A., Liu, Y., Loges, N.T., Pathak, N., Austin-Tse, C., Sheridan, E., Schmidts, M. *et al.* (2012) CCDC103 mutations cause primary ciliary dyskinesia by disrupting assembly of ciliary dynein arms. *Nat Genet*, **44**, 714-719.

42 Jordan, D.M., Frangakis, S.G., Golzio, C., Cassa, C.A., Kurtzberg, J., Task Force for Neonatal, G., Davis, E.E., Sunyaev, S.R. and Katsanis, N. (2015) Identification of cis-suppression of human disease mutations by comparative genomics. *Nature*, **524**, 225-229.

43 Li, H. and Durbin, R. (2009) Fast and accurate short read alignment with Burrows-Wheeler transform. *Bioinformatics*, **25**, 1754-1760.

44 DePristo, M.A., Banks, E., Poplin, R., Garimella, K.V., Maguire, J.R., Hartl, C., Philippakis, A.A., del Angel, G., Rivas, M.A., Hanna, M. *et al.* (2011) A framework for variation discovery and genotyping using next-generation DNA sequencing data. *Nat Genet*, **43**, 491-498.

45 Li, H., Handsaker, B., Wysoker, A., Fennell, T., Ruan, J., Homer, N., Marth, G., Abecasis, G., Durbin, R. and Genome Project Data Processing, S. (2009) The Sequence Alignment/Map format and SAMtools. *Bioinformatics*, **25**, 2078-2079.

**Figure Legends**

**Figure 1: Pedigree and molecular analysis of affected individuals**

**(A)** Pedigrees of both families, indicating segregation of the *CCDC32* variant in each family (c.54dupT in Family A, and c.189_190dupGG in Family B). **(B)** Sanger traces of individuals with homozygous (upper panels) and heterozygous (lower panel) *CCDC32* variants.
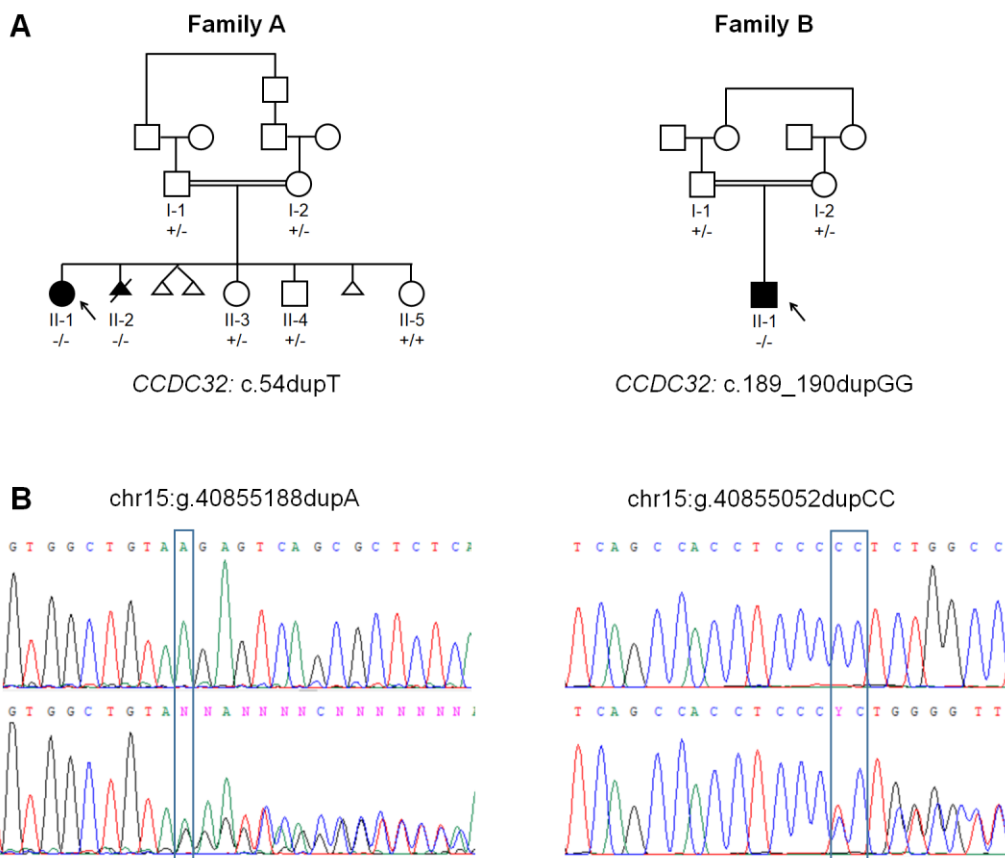
**Figure 2. *ccdc32* depletion impairs craniofacial and neural development in zebrafish.**

(**A**) Quantification of head size in *ccdc32* depleted embryos. (**B**) Representative ventral images of 3dpf uninjected control (UC), sgRNA1 only (100 pg gRNA), and sgRNA1 & Cas9 injected -*1.4col1a1:egfp* zebrafish larvae are shown in panels on left. Anterior is to the left. Dotted yellow line represents ceratohyal angle. Graph displays quantitative assessment of the CH angle following injection of either sgRNA + Cas9. (**C**) Representative dorsal images of anti-acetylated-tubulin stained embryos. Cerebellum is indicated with a red arrow in UC image. Cerebellar size is reduced in *ccdc32* crispants. In all graphs the data are represented as the mean ±s.e.m.; *$P<0.05$, **$P<0.01$, ***$P<0.001$ and ****$P<0.0001$ vs uninjected controls. Tukey's test was applied following a significant one-way ANOVA.

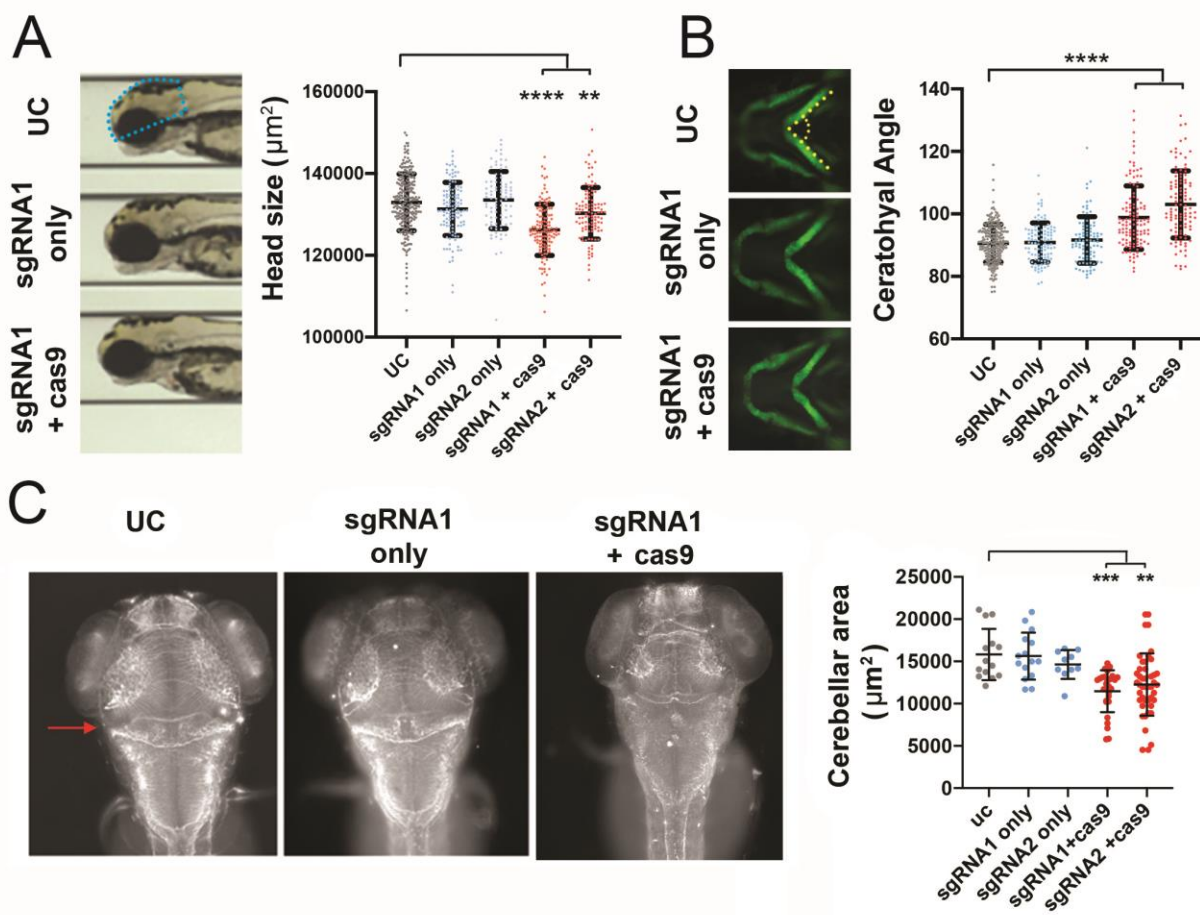**Figure 3. *ccdc32* is required for left – right development in zebrafish.**

**(A)** Representative images of normal, midline and reversed cardiac looping in control and *ccdc32* depleted embryos. Graph displays % of embryos with each phenotype following injection with either sgRNA in the presence or absence of Cas9. **(B)** Sided expression of *spaw* is abnormal in ccdc32 targeted embryos. *spaw* is normally expressed on the left. Depletion of *ccdc32* results in abnormal bilateral or right sided expression.
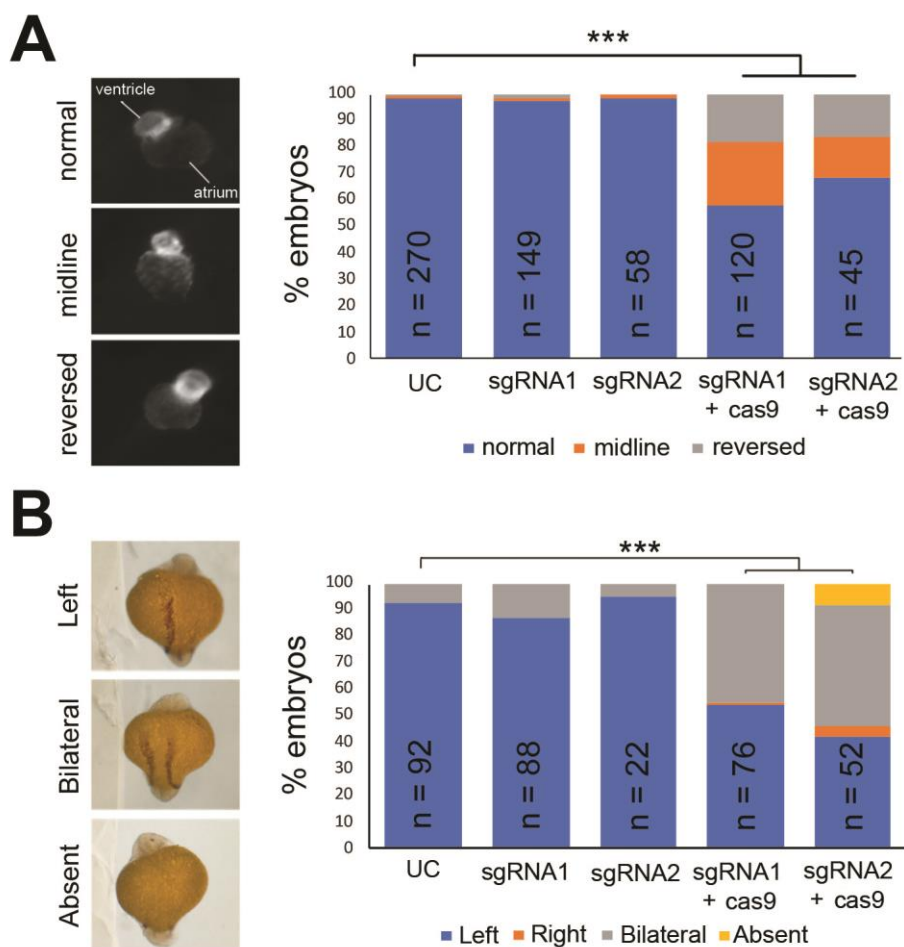
**Figure 4. Cilia formation is impaired by *ccdc32* depeletion**

(**A**) The number and length of cilia in Kupffers vesicle is decreased following *ccdc32* depletion. Representative images of cilia in the KV of uninjected control, sgRNA1 only, and sgRNA1 + Cas9 injected embryos assayed by IF using anti α-acetylated tubulin antibody. Graphs describe the quantification of cilia number and length in each experimental condition. The data are represented as the mean ±s.e.m.; *$P<0.05$, and ***$P<0.001$ vs uninjected controls. Tukey's test was applied following a significant one-way ANOVA. (**B**) Representative images from GFP-labelled cilia in control and si*Ccdc32* cells. scale: 20um; inset scale: 5um. Graph on lower left depicts reduction of *Ccdc32* expression as assayed by qRT-PCR (mean ±s.e.m.). Middle and right graphs quantify % of ciliated cells (mean ±s.e.m.) and cilia length (mean ±s.d.), respectively. Statistical significance is calculated by t-test. *$P<0.05$, **$P<0.01$, and ***$P<0.001$.

# A

## KV cilia



α-tubulin | UC | sgRNA1 | sgRNA1 + cas9



# B

## mIMCD3 5-HT6-GFP



siControl | siCcdc32